Materials Science and Engineering, A130 (1990) 101–111

Microstructure and Stability of Fe–Cr–C Hardfacing Alloys

S. ATAMERT and H. K. D. H. BHADESHIA

Department of Materials Science and Metallurgy, University of Cambridge, Pembroke Street, Cambridge CB2 3QZ (U.K.)

(Received March 26, 1990)

Abstract

The microstructure and high temperature stability of an iron-based hardfacing alloy of nominal composition Fe–30Cr–3.8C (weight per cent) deposited by manual metal arc welding has been investigated using microscopy, microanalysis, dilatometry and thermodynamic modelling. In the as-deposited condition the undiluted alloy was confirmed to consist of a mixture of M_7C_3 carbide and metastable austenite containing a high chromium concentration. Since the properties of the alloy can depend on the stability of the austenite, annealing experiments were carried out to investigate the decomposition of the austenite into a mixture of ferrite and carbides. The results demonstrate that at temperatures around 750 °C the austenite starts to decompose rapidly, beginning with the precipitation of $M_{23}C_6$ carbides, although the final equilibrium phase mixture is simply chromium-depleted ferrite and M_7C_3. The implications of these results are discussed with respect to the potential applications of the alloy.

1. Introduction

Iron-based alloys with substantial concentrations of chromium and carbon and a microstructure containing a large volume fraction of hard alloy carbides are often used for cladding surfaces subject to abrasion or other kinds of wear, sometimes at elevated temperatures [1, 2]. The chromium concentration can be up to 40 wt.% and the carbon concentration up to 6 wt.%. The alloys are often deposited by arc welding in which case the cooling rates can be sufficiently large (20–30 K s^{-1}) to give a non-equilibrium microstructure of M_7C_3 carbides (where the "M" refers to metal atoms) in a matrix of metastable austenite. Because the austenite is retained from a very high temperature where its equilibrium chromium concentration can be as high as 16 wt.% [3, 4], it is expected to be resistant to corrosion. If the austenite subsequently transforms into an equilibrium mixture of ferrite and more M_7C_3 carbides, the much lower chromium concentration in the resulting ferrite is inadequate to support a continuous Cr_2O_3 film, so that the corrosion resistance of the matrix phase is then expected to decrease. The purpose of the present work was therefore to extend some earlier work [3] on an Fe–Cr–C hardfacing alloy to a leaner commercial alloy, with the specific aim of investigating the stability of its microstructure to annealing heat treatments, using microscopy, microanalysis, dilatometry and thermodynamic modelling.

2. Experimental techniques

The hardfacing alloys were deposited using manual metal arc welding in three layers so that the top layer could be examined without the influence of significant dilution effects due to mixing with the mild steel baseplate. The electrodes used were 4 mm in diameter, welded at 160 A, 23 V a.c. and a welding speed of 4 mm s^{-1}. The interpass temperature was 350 °C. The chemical compositions (weight per cent) of the top layers were spectroscopically measured to be Fe–29.19Cr–1.32Mn–0.59Si–0.01Mo–3.8C in alloy 1 and Fe–37.87Cr–4.5C–1.41Mn–0.86Si in alloy 2. Since the dilatometric experiments are carried out in alloy 1 and since it also contains substantially lower chromium and carbon concentrations relative to the alloy investigated earlier [3], it was felt necessary to repeat some of the initial characterization experiments to confirm the starting microstructure.

Thin foil specimens for transmission electron microscopy were prepared from discs 0.25 mm thick spark machined from the top layer of the weld. The discs were thinned further by abrasion and were then electropolished using a 5%

0921-5093/90/$3.50

perchloric acid, 25% glycerol and 70% ethanol mixture at ambient temperature and 55 V polishing potential. The foils were examined using a Philips EM400T transmission electron microscope operated at 120 kV. Microanalytical experiments were also carried out on this microscope using an energy dispersive X-ray (EDX) analysis facility. The specimens, which were about 100 nm thick, were held in a beryllium holder tilted 35° from the normal, which is equal to the take-off angle. The X-ray count rate was optimized at about 900 counts s^{-1}, giving a statistical accuracy of about ± 1 wt.%. The data were analysed using the LINK RTS 2 FLS programme for thin foil microanalysis; this corrects the data for atomic number and absorption and accounts for overlapping peaks by fitting standard profiles. Even though the probe diameter used was about 3 nm, beam spreading due to the scattering of electrons with the thin foil gave an estimated broadened beam diameter of about 20 nm. The elements analysed were iron, silicon, chromium and manganese; at typical levels found in the sort of alloy studied here, it has been established [3] that fluorescence effects in the thin foil can be neglected.

The microanalytical data reported for the primary carbides and for the regions close to the primary carbides were obtained using an EDX analysis system on a scanning electron microscope, with the data fully corrected for absorption, atomic number and fluorescence.

The beryllium window on all the EDX systems used in the present work prevents the detection of light elements such as carbon. Consequently, the concentration Y_i for element i is intended to refer to the atomic per cent of i if the presence of carbon is neglected, whereas the true concentration is denoted V_i in units of atomic per cent. To calculate V_C, the carbon concentration of M_7C_3 was calculated assuming stoichiometry and that of austenite was measured using X-ray diffractometry (step scanning at 0.02° 2θ intervals for the range $2\theta = 10°–120°$ with Cu Kα X-radiation) via the change in the austenite lattice parameter a_γ due to the solution of carbon and other elements [5]:

$$a_\gamma \simeq 0.3577 + 0.00065\mathrm{C} + 0.0001\mathrm{Mn} + 0.00006\mathrm{Cr} - 0.00002\mathrm{Ni} + 0.00053\mathrm{Mo} \quad (\mathrm{nm}) \qquad (1)$$

where the concentrations of the solutes are given in atomic per cent. Having estimated V_C in this way, the true concentrations of the other elements can be obtained as follows:

$$V_i = Y_i(1 - 0.01\,V_C) \qquad (2)$$

Specimens for dilatometry were, after machining from the top layer, electroplated with layers of nickel to avoid surface degradation and nucleation during heat treatment. The dilatometer used was a Theta Industries high speed machine fitted with a radio-frequency furnace of essentially zero thermal mass and interfaced with a computer to collect length, time and temperature data on floppy discs. The experiments simply involved the rapid heating of the as-deposited undiluted samples to an isothermal reaction temperature to study the kinetics of decomposition of metastable austenite.

Thermodynamic calculations to establish the equilibrium (or metastable equilibrium) phase chemistries were carried out in March 1990 using the MTDATA system (Metallurgical and Thermochemical Databank) of the National Physical Laboratory. The components taken into account were iron, chromium, molybdenum, manganese and silicon.

3. Results and discussion

3.1. Metallography

The liquidus projection of the Fe–Cr–C system (Fig. 1 [6]) suggests that solidification in the alloys used begins with the formation of primary M_7C_3 carbides, the residual liquid decomposing eventually by a ternary eutectic reaction into a mixture of austenite and more M_7C_3 carbides. On the other hand, the layer deposited first is diluted heavily by mixing with the mild steel baseplate, so that its microstructure was found to consist largely of primary austenite dendrites instead of the primary M_7C_3 expected in the undiluted alloy (Fig. 2(a)). Some of the austenite dendrites close to the base metal fusion boundary (where dilution is expected to be at a maximum) were found to decompose to plate martensite on cooling to ambient temperature (Figs. 2(a) and 2(b)), and it was also clear that some carbon had diffused into the baseplate beyond the fusion surface (Fig. 2(a)). The microstructure of the undiluted top layer revealed the expected large primary M_7C_3 carbides, which were all found to be surrounded by precipitate-free zones (Fig. 2(c)). These zones are believed to arise due to the depletion of

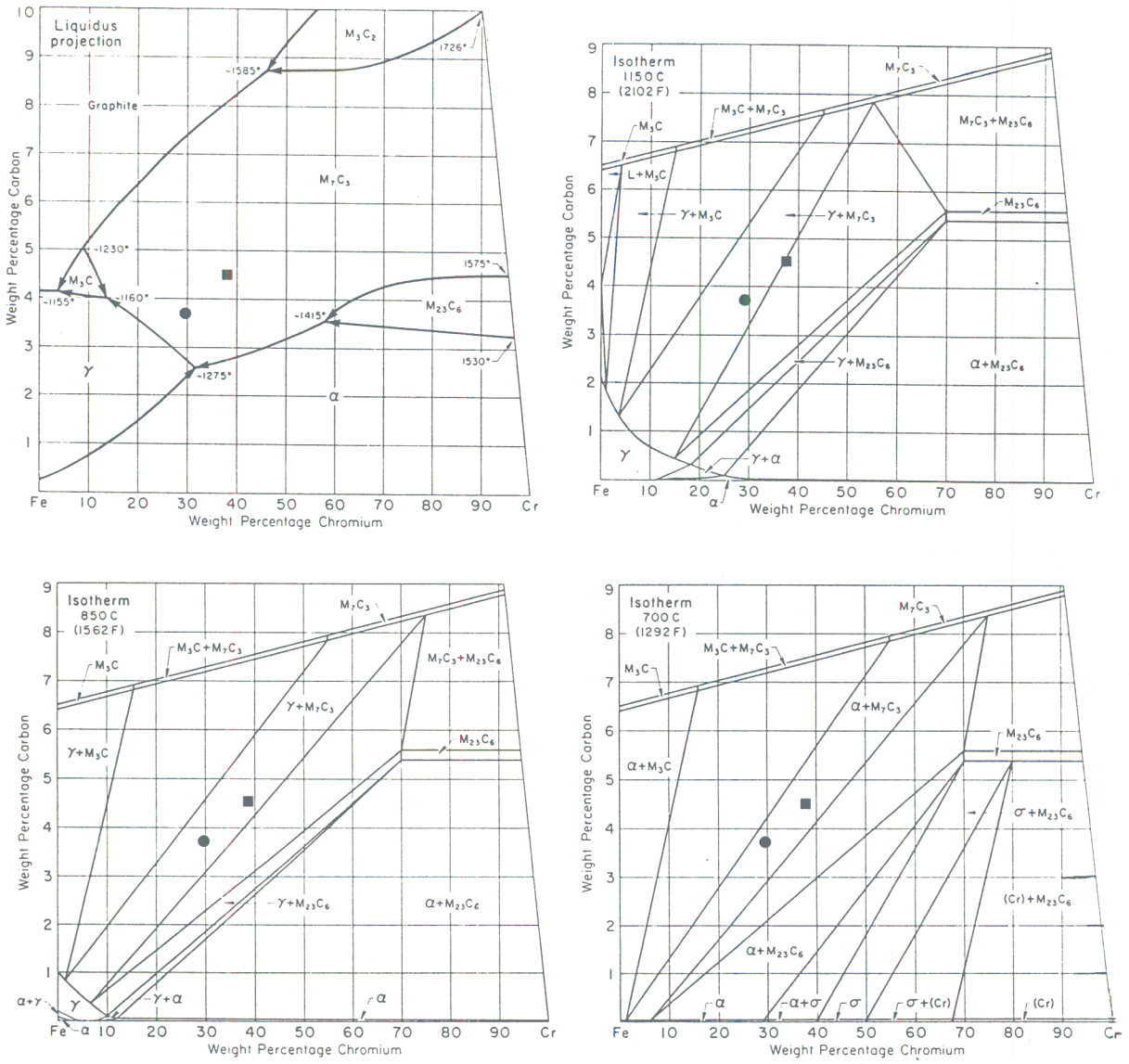

Fig. 1. Liquidus projection and isothermal sections of Fe–Cr–C system [6]. The points indicated on the diagram show the positions of the experimental alloys: ●, alloy 1; ■, alloy 2.

chromium in the liquid close to the primary carbides [3], a factor confirmed in the present work using microanalysis data discussed later in the text. Consistent with previous work [3], transmission electron microscopy (Fig. 3) and X-ray diffraction experiments (Table 1) confirmed that the matrix phase consists of a eutectic mixture of retained austenite and M_7C_3 carbides, in spite of the fact that the equilibrium microstructure below about 700 °C ought to be a mixture of ferrite and a higher volume fraction of M_7C_3 carbides (Fig. 1).

3.2. Microanalysis and thermodynamic analysis

The experimentally measured partition coefficient of chromium, *i.e.* k_{Cr}, given by the ratio of concentration (atomic per cent) in primary M_7C_3 to that in austenite, was measured using microanalysis to be about 3.0. A large concentration of iron was also noted in the M_7C_3 carbides (Fig. 4). Manganese also partitions preferentially into the carbides, although as reported previously, silicon is rejected during the growth of the M_7C_3 carbides. The eutectic carbides have essentially the same chemical composition as the primary

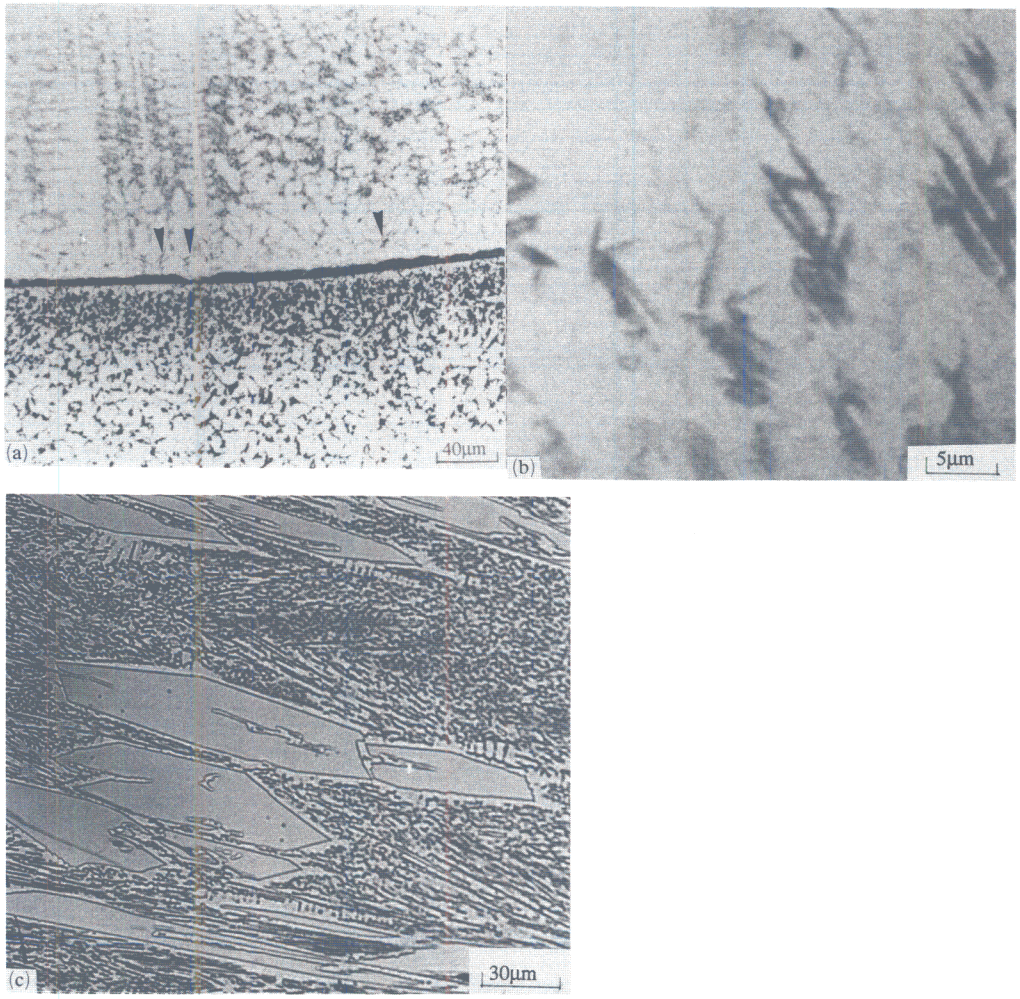

Fig. 2. Optical micrographs of alloy 1. (a) Cross-section showing the highly diluted first layer–base metal interface region, the carbon-enriched area in the substrate along the boundary and dendritic solidification of the first layer of the weld deposit. The arrows indicate regions which have decomposed by martensitic reaction. (b) Higher magnification image showing lenticular martensite observed along the first layer–base metal interface. (c) The top layer consisting of large M_7C_3 carbides surrounded by precipitate-free zones and the eutectic mixture of austenite and M_7C_3 carbides.

carbides, presumably because the microstructure evolves over a fairly narrow temperature range in the vicinity of the solidus temperature. For the same reason, the carbide-free austenite surrounding the primary carbides is found to be similar in composition to the "eutectic austenite". The mean compositions of all the phases, over 15 samples in each case, are given in Table 2.

3.3. *Dilatometry*

Dilatometry was used to follow the decomposition of austenite during annealing of samples machined from the undiluted top layer at 800, 750 and 700 °C. The experiments were carried out by rapidly heating samples from the ambient

TABLE 1 Results from X-ray diffraction experiments on the undiluted layer. The first column represents the interplanar spacings corresponding to the detected peaks and the second column the Miller indices of the planes responsible for those peaks. The indices of the M_7C_3 carbide are stated with respect to the hexagonal cell in three-index notation. Austenite is represented by the symbol γ

Spacing (nm)	*Miller indices*	*Phase*
0.2280	240	M_7C_3
0.2076	111	γ
0.2032	241	M_7C_3
0.1807	002	γ
0.1746	442	M_7C_3
0.1274	220	γ
0.1168	011	M_7C_3
0.1088	472	M_7C_3
0.1042	222	γ

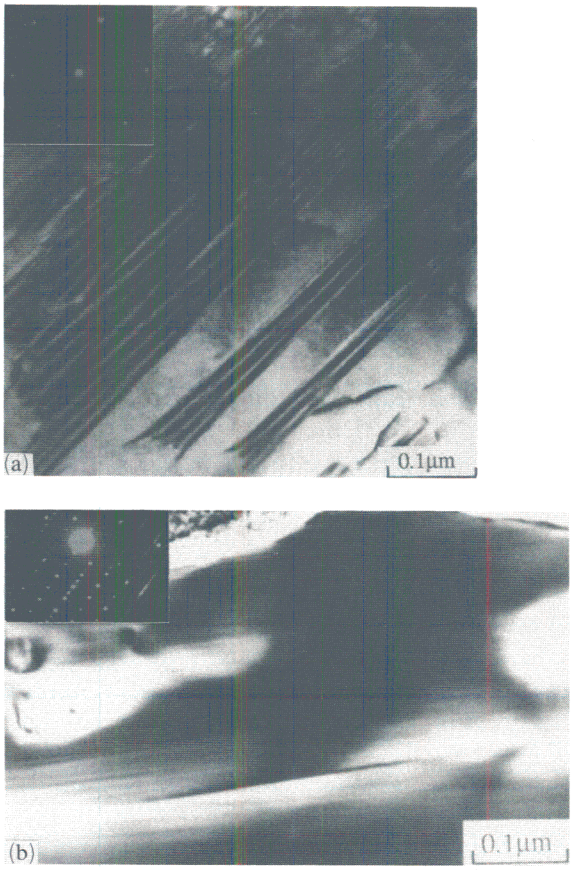

Fig. 3. (a) Transmission electron micrograph of the *metastable* austenitic matrix showing stacking faults (selected area diffraction pattern from the γ is inserted); the zone axis of the pattern is $\langle 114 \rangle_{fcc}$. (b) Transmission electron micrograph of the M_7C_3 carbides; the zone axis of the inserted diffraction pattern is $\langle 111 \rangle_{hcp}$.

TABLE 2 Mean composition (atomic per cent) of the phases in the undiluted layer. The results for the primary carbides and for the austenite in the vicinity of the primary carbides are from microanalytical experiments conducted using a scanning electron microscope. The data have been rounded off to the nearest significant figure. The estimated errors in the data are indicated in Fig. 4

Element	*Primary M_7C_3*	*Austenite near primary M_7C_3*	*Eutectic austenite*	*Eutectic M_7C_3*
Fe	24	76	76	26
Cr	45	15	15	43
Mn	1	1.5	1.5	1
Si	—	2	1.5	—
C	30	6	6	30

temperature to the annealing temperature and holding them there for a prolonged period of time. Thus the data collected consist essentially of dimensional changes occurring at constant tem-

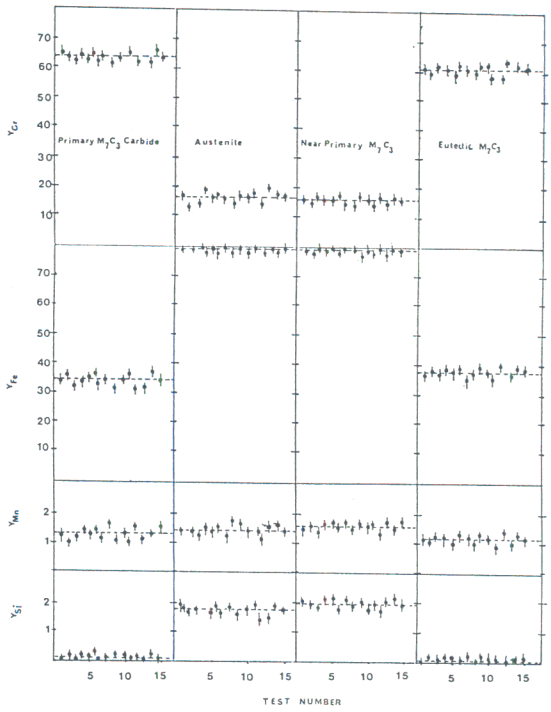

Fig. 4. Microanalytical data on primary M_7C_3, eutectic M_7C_3, near-primary M_7C_3 and austenitic matrix when carbon is not included in the calculations (atomic per cent). The continuous lines show the average values in each phase.

perature due to density changes caused by the transformation of austenite. Since M_7C_3 carbide is non-cubic in crystal structure, dimensional changes during its formation are expected to be anisotropic. It is, however, reasonably assumed that since the carbides are found in many orientations, any dimensional changes are averaged out, thereby giving macroscopically isotropic behaviour. With this assumption in mind, the relative dimensional change $\Delta L/L$ due to the complete decomposition of austenite into a mixture of ferrite and M_7C_3 carbides can be shown to be given by

$$3\frac{\Delta L}{L} \simeq \frac{\Delta V}{V} = \frac{(X_\alpha/2)a_\alpha^3 + \{(X_\gamma - X_\alpha)/56\}Y_{M_7C_3} - (X_\gamma/4)a_\gamma^3}{(X_\gamma/4)a_\gamma^3} \quad (3)$$

where X_α and X_γ represent the mole fractions of metal atoms in ferrite and austenite respectively, L and V represent the specimen length and volume respectively, a_α and a_γ the lattice parameters

of ferrite and austenite respectively, and $Y_{M_7C_3}$ is the volume of the M_7C_3 unit cell containing 56 metal atoms per cell. The ferrite and austenite cells contain 2 and 4 metal atoms per cell respectively. Note that the equation also has the implicit assumption that the compositions of the original and new M_7C_3 carbides are essentially identical. The lattice parameter of each phase has in the above equations to be expressed at the reaction temperature, using relations of the form

$$a_\alpha = \bar{a}_\alpha\{1 + e_\alpha(T-25)\} \quad (4)$$

where T is the temperature in degrees Celsius, $\bar{a}_\alpha$ is the ambient temperature lattice parameter of ferrite and e_α is the thermal expansion coefficient of ferrite. The parameter was measured using the Debye–Scherrer X-ray diffraction technique on a sample which had been annealed for 24 h at 700 °C. The annealing treatment led to the decomposition of austenite to ferrite and carbides; $\bar{a}_\alpha$ was therefore found to be 0.28633 nm. The austenite lattice parameter $\bar{a}_\gamma$ was similarly measured to be 0.362 nm; $\bar{a}_{M_7C_3}$ and $\bar{c}_{M_7C_3}$ are assumed to be 1.377 and 0.444 nm respectively [7]. The expansion coefficients (e) for the three phases were taken from published sources [8, 9].

Equation (3) simplifies if the further assumption is made that mole fractions can be equated to volume fractions:

$$3\frac{\Delta L}{L} \simeq \frac{\Delta V}{V}$$

$$= \frac{(V_\alpha/2)a_\alpha^3 + \{(V_\gamma - V_\alpha)/56\}Y_{M_7C_3} - (V_\gamma/4)a_\gamma^3}{(V_\gamma/4)a_\gamma^3} \quad (5)$$

where V_α and V_γ are the volume fractions of ferrite and austenite respectively.

The dilatometric results presented in Fig. 5 show a net decrease in volume as the austenite transforms to ferrite and M_7C_3. The relative volume change associated with the transformation depends on the volume fraction of austenite found after solidification as seen in eqn. (3). The equilibrium volume fractions of ferrite and M_7C_3 phases below 850 °C are essentially independent of temperature and remain as 0.49 and 0.51 respectively as discussed later in the section on thermodynamic analysis. The overall volume change in the range of 700–800 °C is therefore expected to be similar. Thus the calculated volume changes as a function of initial volume fraction of austenite at 700, 750 and 800 °C were found to be close to each other as shown in Fig. 6. The theory therefore shows that a volume contraction is expected if the austenite volume fraction in the microstructure prior to annealing is lower than about 0.57 (Fig. 6).

The experimental data presented in Fig. 5 represent the first few hours of the reaction at the

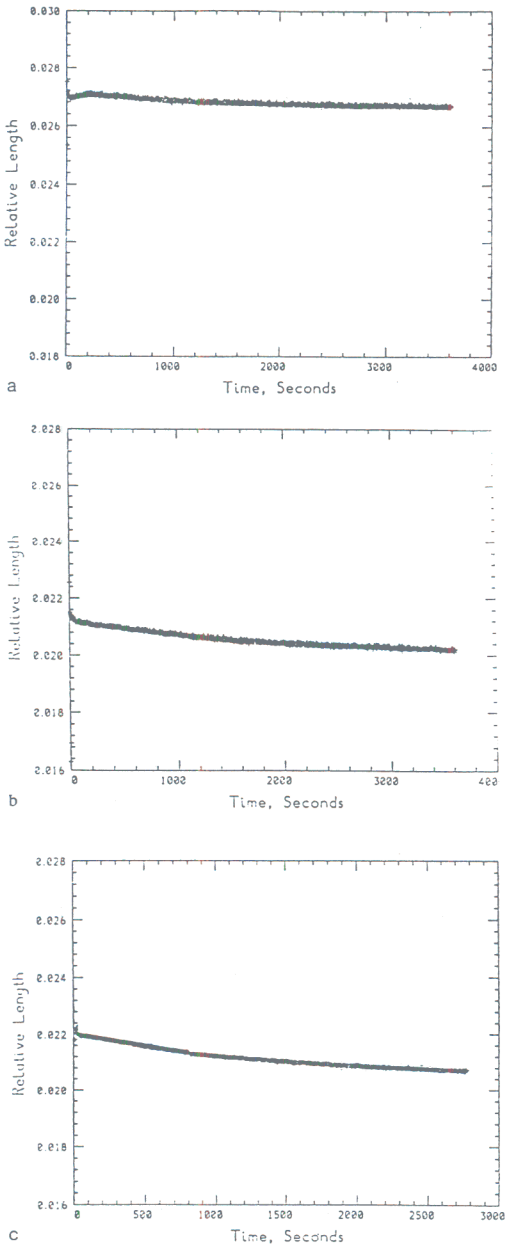

Fig. 5. Relative length change *vs.* time curves at (a) 700; (b) 750 and (c) 800 °C.

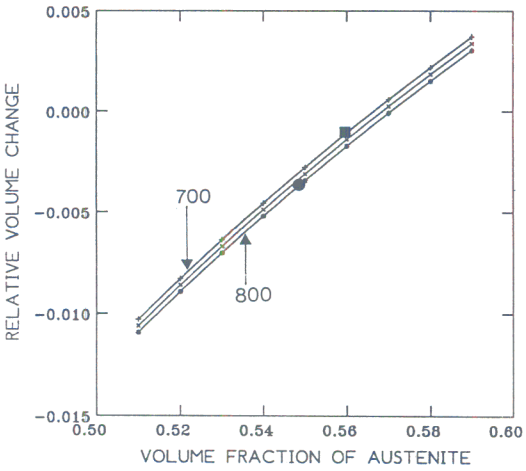

Fig. 6. The calculated overall volume change expected as a function of the volume fraction of austenite at 700, 750 and 800 °C when austenite transforms to $M_7C_3 + \alpha$. The points marked on the lines show the experimentally observed volume contractions (●, 800 and 750 °C; ■, 700 °C), suggesting that the microstructure before the decomposition contains 55% austenite.

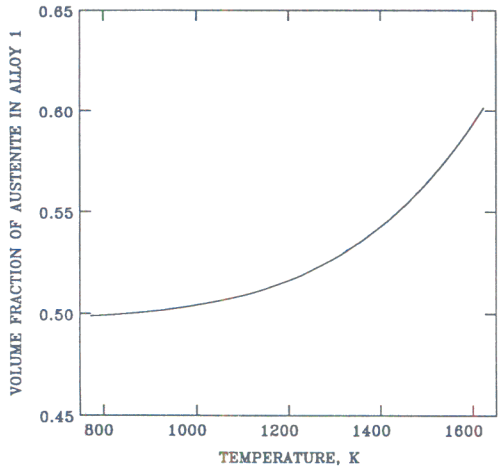

Fig. 7. Thermodynamically calculated volume fraction of austenite in alloy 1 as a function of temperature when γ and M_7C_3 are in equilibrium, with all other phases being suppressed.

annealing temperature and demonstrate that the rate of austenite decomposition can be very rapid at temperatures in the range 750–800 °C. The measured volume contractions at 750 and 800 °C after 3500 s were found to be about 0.004, corresponding to an initial austenite volume fraction of about 0.55 before the transformation (Fig. 6). However, the volume contraction at 700 °C after 4000 s was only 0.0008, suggesting that the reaction rate is relatively slow at this temperature. It is interesting that the 0.55 volume fraction of austenite indicated by the dilatometric data plotted in Fig. 6 is in good agreement with the thermodynamically estimated volume fraction of γ in Fig. 7, assuming that the development of the microstructure during cooling stops at a relatively high temperature of about 1300 °C. As will be seen later in the section on thermodynamic analysis, this is consistent with the observed partitioning of alloying elements between the γ and M_7C_3 phases.

3.4. Metallography of austenite decomposition

Thin foils for transmission electron microscopy were prepared from specimens quenched to ambient temperature after holding at the annealing temperature for a variety of time intervals.

Surprisingly, the first reaction that was found to occur after 100 s at 750 °C involved the precipitation of fine particles of $M_{23}C_6$ in a cube–cube orientation relationship with respect to the austenite (Fig. 8). $M_{23}C_6$ has a cubic F lattice with a lattice parameter which is about three times that of austenite, and the cube–cube orientation relationship is the one normally observed between this carbide and austenite. The $M_{23}C_6$ carbide is not a thermodynamically stable phase for this alloy (as is evident from the phase diagrams, Fig. 1). The preferential nucleation of these carbides over the equilibrium M_7C_3 could be associated with the good lattice matching between the austenite and $M_{23}C_6$ phases which would tend to reduce the interfacial energy and hence the activation energy for nucleation.

Further holding at 750 °C for 24 h led to the replacement of austenite with ferrite, and the only carbides that could be found were extremely fine and numerous precipitates of M_7C_3 carbides (Fig. 9). The austenite decomposition reaction was manifested in optical micrographs by a distinct change in the etching characteristics of the matrix phase; the previously light-etching austenite matrix very clearly appeared dark and speckled after the decomposition (Fig. 10).

3.5. Thermodynamic analysis

Figure 11 illustrates the thermodynamically calculated volume fractions of phases expected under equilibrium conditions in alloys 1 and 2. The calculations were carried out by minimizing the Gibbs free energy of austenite, ferrite and M_7C_3 carbide for alloys containing carbon, iron,

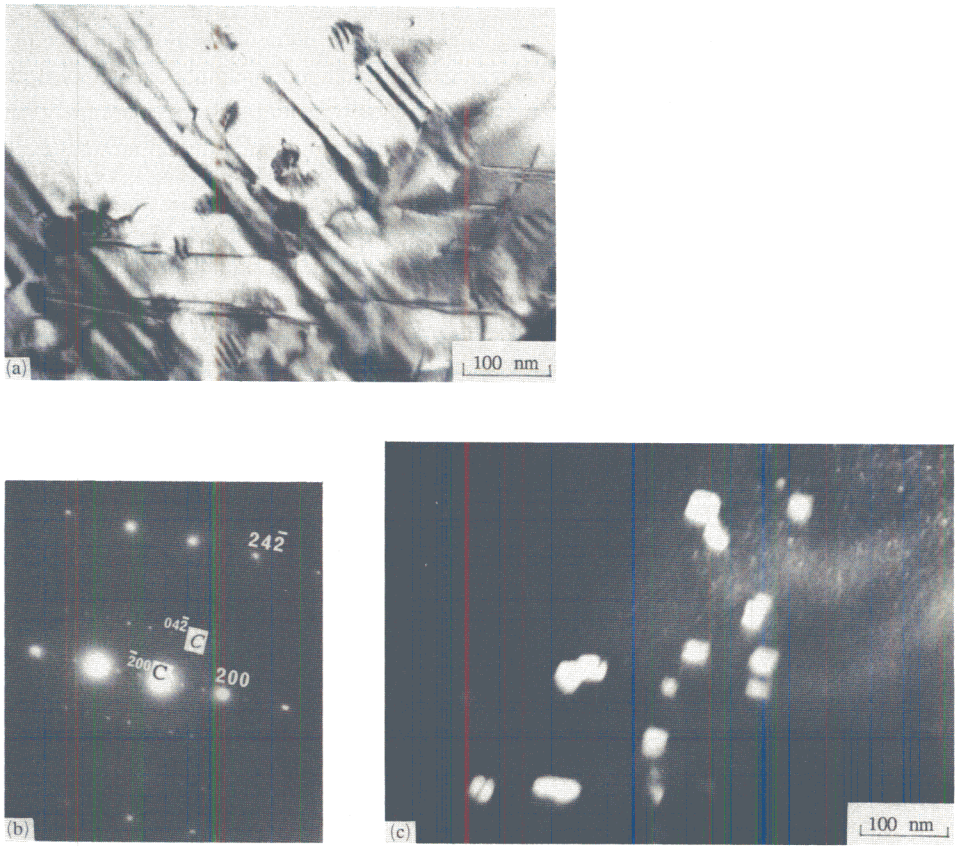

Fig. 8. (a) Bright field transmission electron micrograph after 100 s at 750 °C. (b) Corresponding electron diffraction pattern showing $[012]_{\gamma}//[012]_{M_{23}C_6}$ zone axis with a cube–cube orientation relationship. (c) Corresponding dark field image using (242) carbide reflection.

silicon, molybdenum, manganese and chromium. It is evident that the results differ significantly from those expected from an interpretation of the Fe–Cr–C ternary phase diagram (Fig. 1). The latter indicates that only austenite and M_7C_3 should be stable at elevated temperatures in excess of about 700 °C. Figure 11, on the other hand, shows that austenite is never the stable phase in alloy 2, the equilibrium microstructure consisting of just ferrite and M_7C_3 in its solid state. Furthermore, ferrite is always found to coexist at equilibrium with austenite above 827 °C in alloy 1.

In spite of these results, metallography has shown conclusively that both alloys in practice solidify to a microstructure consisting of a mixture of metastable austenite and M_7C_3, providing strong evidence that the austenitic phase must be kinetically favoured during solidification. In fact, there are many examples of such phenomena reported in the literature, which has been reviewed by Fredricksson [10], where although ferrite may represent the thermodynamically stable phase, solidification under non-equilibrium cooling conditions leads instead to the kinetically favoured austenite, and the present results support these general observations.

The conclusion drawn in earlier work [3] in which the data were interpreted using the Fe–Cr–C ternary phase diagram, *i.e.* that the experimental alloy first solidifies to an *equilibrium* mixture of austenite and M_7C_3, is therefore not justified. To investigate why the thermodynamic calculations here differ so markedly from the predictions of the Fe–Cr–C ternary phase diagram, the concentrations of the other solute elements were varied. It was found that the system is rather sensitive to silicon concentration. For example, in alloy 2, which has the higher

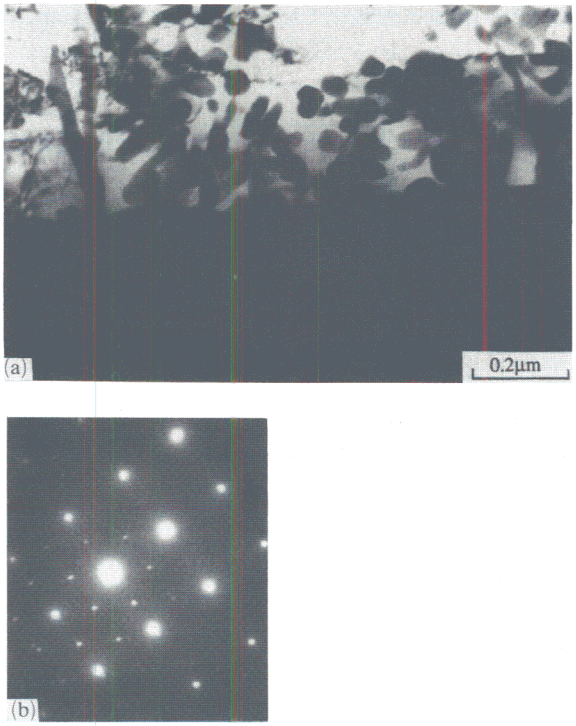

Fig. 9. Bright field transmission electron micrograph after 24 h at 750 °C showing the transformation products of ferrite and fine M_7C_3 carbides; the dark region in the lower part of the micrograph is a primary M_7C_3 carbide. (b) Corresponding electron diffraction pattern showing $\langle 100\rangle_\alpha // \langle 001\rangle_{M_7C_3}$ orientation relationship.

silicon concentration, removal of silicon makes the mixture of austenite and M_7C_3 thermodynamically stable at temperatures above approximately 800 °C, consistent with the ternary Fe–Cr–C phase diagram, with ferrite and M_7C_3 being the stable phases at lower temperatures. If the ferrite phase is suppressed in the calculations, to simulate the kinetic advantage of austenite, then the austenite and M_7C_3 mixture remains stable at all temperatures. Of course, when an amount of silicon consistent with the composition of alloy 2 is added, the equilibrium mixture is one of ferrite and M_7C_3 at all temperatures.

Thus silicon has a powerful effect on alloys of the kind studied here; although added in relatively low concentrations to deoxidize the weld metal, its effect is multiplied since both experiment and our thermodynamic calculations show that it has negligible solubility in M_7C_3, so that almost all of it ends up in the enriched residue. The higher stability of austenite in alloy 1 is consistent with its lower overall silicon concentration.

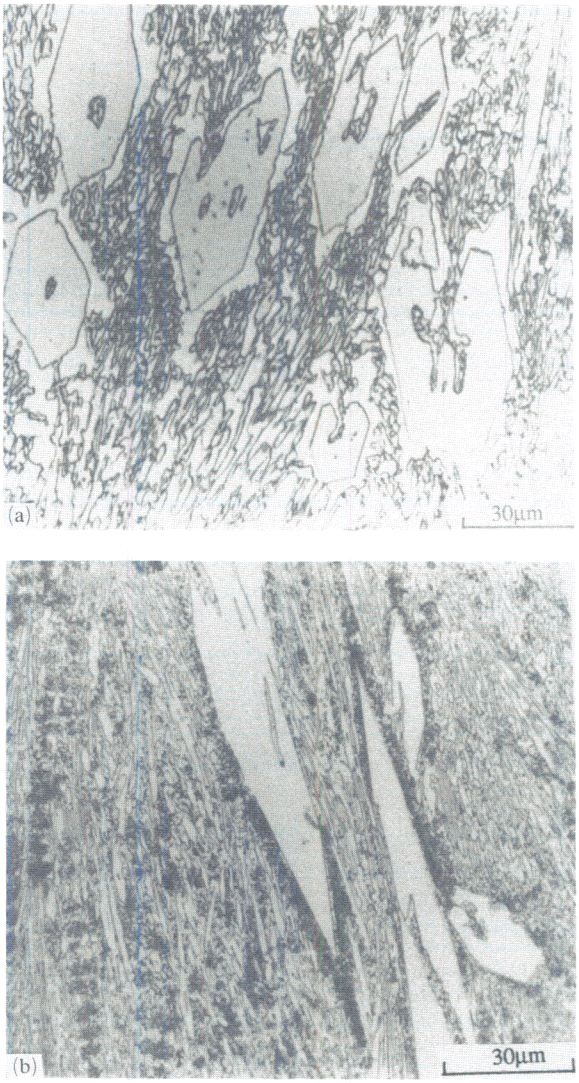

Fig. 10. Optical micrographs, (a) before the transformation and (b) following transformation of austenite, after isothermal treatment for 24 h at 750 °C. Note the change in etching contrast associated with the decomposition of the austenite.

It has already been pointed out that the partition coefficient k_{Cr} representing the ratio of chromium concentration in M_7C_3 to that in austenite was found to be about 3.0. Figure 12 shows thermodynamically calculated values of the partition coefficient for alloy 1 when the formation of ferrite is suppressed. Comparison of the calculations with the experimental value of $k_{Cr} \simeq 3.0$ indicates that the phase compositions do not change significantly during cooling below about 1300 °C. In this sense the phase chemistries are *frozen* immediately after solidification is

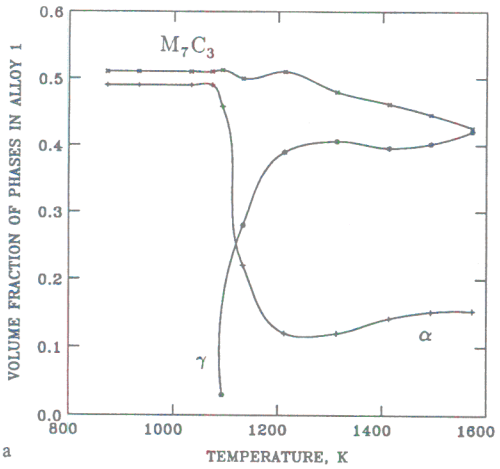

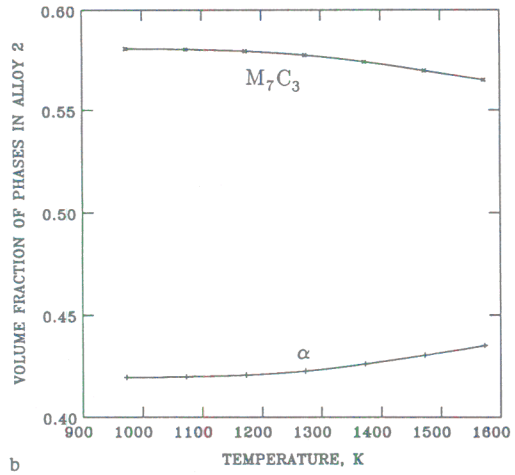

Fig. 11. Calculated equilibrium volume fractions of phases as a function of temperature in (a) alloy 1 and (b) alloy 2.

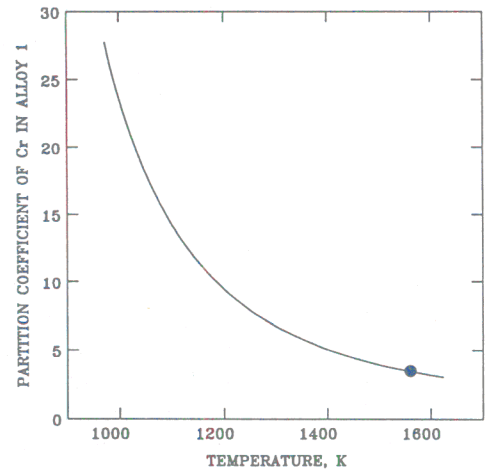

Fig. 12. Variation of the partitioning coefficient of chromium (the ratio of atomic per cent of chromium in carbide to that in austenite) as a function of temperature in alloy 1. The point shows the experimentally measured partition coefficient of chromium, indicating that the microstructure evolved with non-equilibrium solidification conditions.

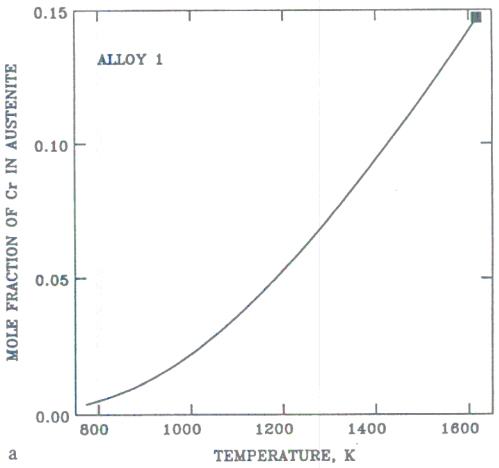

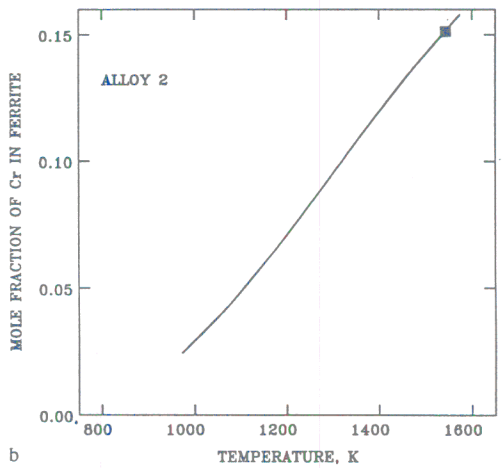

Fig. 13. Calculated chromium concentration in the matrix phase as a function of temperature in (a) alloy 1 and (b) alloy 2. The points show the experimentally measured values.

completed, a consequence of the non-equilibrium high cooling rates associated with arc welding. This is consistent with the dilatometrically estimated austenite volume fraction of 0.55, which compares with the value of 0.57 expected at 1300 °C. This hypothesis is also consistent with the measured mole fractions of chromium in the matrix phases and iron and chromium in M_7C_3 in both alloys 1 and 2 (Figs. 13 and 14).

The surprising result that $M_{23}C_6$ carbide precipitated first from austenite during tempering at 700 °C can also be examined using the thermodynamic method. The composition (weight per cent) of the austenite that undergoes tempering is given approximately by Fe–16Cr–1.0C–1.40Mn–3.2Si. For that composition, austenite and $M_{23}C_6$ were found to be the equilibrium phases for $T > 702$ °C when the formation of

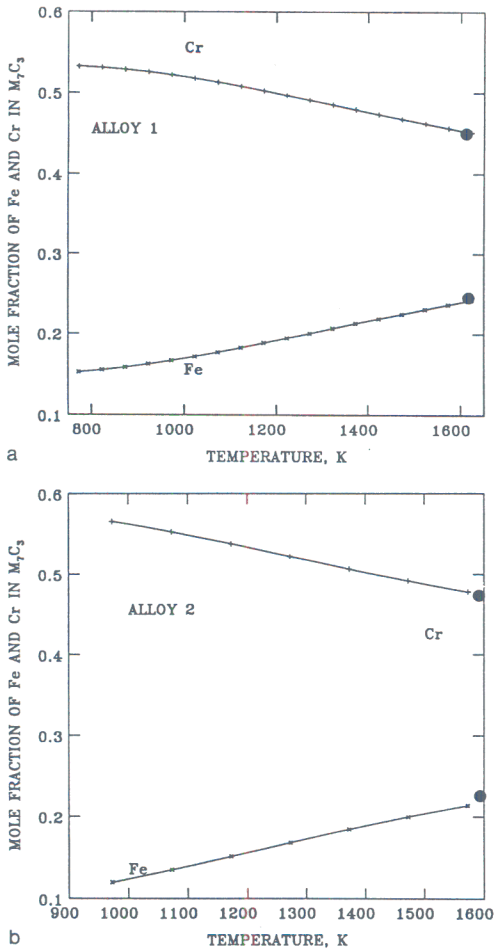

Fig. 14. Calculated chromium and iron concentrations in M_7C_3 as a function of temperature in (a) alloy 1 and (b) alloy 2. The points show the experimentally measured values.

ferrite was suppressed while examining the stability of mixtures of austenite, M_7C_3 and $M_{23}C_6$. This confirms that $M_{23}C_6$ forms only because it has a kinetic advantage relative to the precipitation of ferrite. It is to be expected that when the microstructure is tempered at low temperatures, metastable $M_{23}C_6$ will form and survive until it is replaced eventually by the thermodynamically stable M_7C_3 carbides.

4. Conclusions

The metastable mixture of M_7C_3 carbides and austenite obtained by depositing a hardfacing alloy of approximate composition Fe–30Cr–3.8C (weight per cent) using a manual metal arc-welding technique is found to transform readily into a more stable microstructure consisting of just ferrite and M_7C_3 carbides. However, the decomposition of the austenite appears to occur in two stages, the first involving the formation of $M_{23}C_6$ particles which are in cube–cube orientation with the austenite in which they precipitate. The austenite then decomposes completely to the equilibrium mixture of ferrite and M_7C_3 carbides, the $M_{23}C_6$ particles appearing to dissolve.

Thermodynamic analysis has confirmed these observations and revealed that the alloys should really contain ferrite at all temperatures below the solidus. The fact that they do not seems to be related to some kinetic advantage that the austenite has during solidification. This is consistent with the trends reported in the published literature. Silicon is found to have a major effect on the relative stabilities of austenite and ferrite in the microstructure; relatively small concentrations can render the austenite unstable over the entire temperature range below the solidus temperature. The other observations, on the metastable formation of $M_{23}C_6$ carbides, can also be understood using the thermodynamic method.

Acknowledgments

The authors are grateful to Professor D. Hull for the provision of laboratory facilities at the University of Cambridge, to B. Gretoft, L.-E. Svensson and B. Ulander for valuable discussions and to ESAB AB (Sweden) for the provision of samples. Financial support from the Turkish Government is also gratefully acknowledged.

References

1 *Metals Handbook*, Vol. 6, *Welding, Brazing and Soldering*, American Society for Metals, Metals Park, OH, 9th edn., 1983, pp. 771–803.
2 J. Dodd, *J. Mater. Energy Syst., 2* (1980) 65.
3 L. E. Svensson, B. Gretoft, B. Ulander and H. K. D. H. Bhadeshia, *J. Mater. Sci., 21* (1986) 1015–1019.
4 S. Atamert and H. K. D. H. Bhadeshia, *Trends in Welding Research Symp. Proc., Gatlinburg, TN, May 14–18, 1989*, ASM International, Metals Park, OH, 1990, pp. 273–277.
5 D. J. Dyson and B. Holmes, *J. Iron Steel Inst., 208* (1970) 469–474.
6 *Metals Handbook*, Vol. 8, *Metallography and Phase Diagrams*, American Society for Metals, Metals Park, OH, 8th edn., 1973, p. 402.
7 D. J. Dyson and K. W. Andrews, *J. Iron Steel Inst., 207* (1969) 208–219.
8 V. M. Ershov, *Steel in the USSR, 8* (1984) 101.
9 H. Stuart and N. Ridley, *J. Iron Steel Inst., 204* (1966) 711–717.
10 H. Fredricksson, *Scand. J. Metall., 5* (1976) 27–32.